

Full length article

# Study of point defects diffusion in nickel using kinetic activation–relaxation technique

Sami Mahmoud<sup>\*</sup>, Mickaël Trochet, Oscar A. Restrepo, Normand Mousseau<sup>\*</sup>

Département de physique and Regroupement québécois sur les matériaux de pointe, Université de Montréal, C.P. 6128, Succursale Centre-Ville, Montréal, H3C 3J7, Québec, Canada

## ARTICLE INFO

## Article history:

Received 3 August 2017  
 Received in revised form  
 27 October 2017  
 Accepted 9 November 2017  
 Available online 14 November 2017

## Keywords:

Nickel  
 Self-defect  
 Kinetic Activation Relaxation Technique  
 Diffusion mechanisms  
 Energy landscape

## ABSTRACT

Point defects play a central role in materials properties. Yet, details regarding their diffusion and aggregation are still largely lacking beyond the monomer and dimer. Using the kinetic Activation Relaxation Technique (k-ART), a recently proposed off-lattice kinetic Monte Carlo method, the energy landscape, kinetics and diffusion mechanisms of point defect in fcc nickel are characterized, providing an exhaustive picture of the motion of one to five vacancies and self-interstitials in this system. Starting with a comparison of the prediction of four empirical potentials — the embedded atom method (EAM), the original modified embedded atom method (MEAM1NN), the second nearest neighbor modified embedded atom method (MEAM2NN) and the Reactive Force Field (ReaxFF) —, it is shown that while both EAM and ReaxFF capture the right physics, EAM provides the overall best agreement with *ab initio* and molecular dynamics simulations and available experiments both for vacancies and interstitial defect energetics and kinetics. Extensive k-ART simulations using this potential provide complete details of the energy landscape associated with these defects, demonstrated a complex set of mechanisms available to both vacancies and self-interstitials even in a simple environment such as crystalline Ni. We find, in particular, that the diffusion barriers of both vacancies and interstitials do not change monotonically with the cluster size and that some clusters of vacancies diffuse more easily than single ones. As self-interstitial clusters grow, moreover, we show that the fast diffusion takes place from excited states but ground states can act as pinning centers, contrary to what could be expected.

© 2017 Acta Materialia Inc. Published by Elsevier Ltd. All rights reserved.

## 1. Introduction

Point defects play an important role in materials science as their presence can affect physical and mechanical properties such as electron mobility, conductivity, ductility, strain resistance and more [1,2]. Yet, in spite of their importance, many details are still missing regarding the simplest atomistic mechanisms such as those involving point defect diffusion, mobility and clustering.

Because following the kinetics at this level is difficult experimentally, we have to rely largely on computational approaches to capture the atomic details of these mechanisms. For this, however, we need a proper description, using either *ab initio* approaches or accurate empirical potentials, as well as comprehensive sampling

methods [3]. For full benefits, these two requirements must be brought together as only comprehensive sampling methods can make good use of high quality physical description and vice versa. Such requirements are easier stated than realized, however, as *ab initio* methods are too costly to apply to large systems, preventing extensive strain-free sampling, while empirical potentials, fitted to a small number of properties, often lack in accuracy when applied to generic configurations or non-tested mechanisms.

We are interested, here, in fully characterizing the energy landscape and kinetics of small assemblies of self-defects in the simple bulk fcc Ni systems. To realize this study on the required scale, the use of *ab initio* approaches is not feasible so it is necessary to turn to empirical potentials developed for Ni crystalline environment.

Much effort has gone, over the years, into developing general empirical potentials for such simple fcc metals [4]. Daw and Baskes proposed, many decades ago [5,6], a semi-empirical approach based on Rose's universal scaling law [7], that attempts to replicate, at the classical level, some features of the electronic density

<sup>\*</sup> Corresponding authors.

E-mail addresses: [sami.mahmoud@umontreal.ca](mailto:sami.mahmoud@umontreal.ca) (S. Mahmoud), [mickaël.laurent.trochet@umontreal.ca](mailto:mickaël.laurent.trochet@umontreal.ca) (M. Trochet), [ores77@gmail.com](mailto:ores77@gmail.com) (O.A. Restrepo), [normand.mousseau@umontreal.ca](mailto:normand.mousseau@umontreal.ca) (N. Mousseau).

interaction. Over the years, a number extensions to EAM were introduced. For example, a supplementary angular term has been added to describe non-fcc metals, leading to the modified embedded-atom method (MEAM) [8–11]. The original MEAM formalism works very well for a large range of materials but suffers from various structural instabilities and a fundamental difficulty in reproducing surface reconstructions. Lee *et al* [12–14] introduced a modification of the original MEAM formalism to extend the range of the potential and the many-body screening, leading to the second nearest-neighbor MEAM (MEAM2NN), that describes correctly physical properties of many materials. More recently, a totally different approach was taken to develop a framework for a universal empirical potential that incorporates a bond-order approach and a self-coherent charge distribution [15]. Over the last decade, the Reactive Force Field (ReaxFF) has received considerable interest due to its flexibility and its overall excellent capacity at reproducing physical properties [16,17].

While some of these potentials have been out for a long time, they have not been extensively compared on their capacity at describing self-defects thermodynamic and kinetic properties. Because defect kinetics can be relatively slow, standard methods such as molecular dynamics are not ideal for comparing these various models. This is why we turn, here, to the kinetic Activation-Relaxation Technique (k-ART), a unique off-lattice kinetic Monte-Carlo algorithm with on-the-fly cataloging [18,19]. K-ART has been shown to provide efficient and extensive sampling of energy landscapes as it incorporates exactly all elastic effects at both minima and saddle points for a precise kinetic description of complex materials ranging from defects in metals to long-time evolution of amorphous materials [20–24].

In this paper, we use k-ART to compare self-defect formation energy and diffusion properties of five vacancies and interstitials in nickel, a simple fcc metal, using four empirical potentials: EAM, MEAM1NN, MEAM2NN and ReaxFF. Assessing these four potentials for the one and two vacancies and one self-interstitial atom (SIA) systems, we find that both EAM and ReaxFF recover the fundamental physical properties obtained experimentally or predicted by *ab initio* calculations. Results obtained using EAM, however, are in overall better agreement with experiment results than those obtained with ReaxFF. Focusing on EAM, we characterize the diffusion mechanisms and pathways for small self-defect aggregates, providing a complete picture of the fundamental diffusion mechanisms in nickel and identifying a number of mechanisms that had not be observed before. Moreover, we show that diffusion of vacancy clusters is faster than single vacancy, even for relatively large clusters, although the trend is not monotonic. For interstitials, the situation is more complex and we demonstrate that the diffusion direction is affected by the clusters size confirming recent experiment analysis [25].

## 2. Methods

### 2.1. Potentials

To facilitate the comparison of the effects of various forcefields on the defect kinetics in Ni, we use a version of k-ART coupled to the LAMMPS (Large-scale Atomic/Molecular Massively Parallel Simulator) library [26]. Four Ni potentials are considered in this study: the Embedded Atom Method (EAM), the original Modified Embedded Atom Method (MEAM), the MEAM based on the second-neighbor formalism (2NN) and the Reax forcefield (ReaxFF). EAM parameters are those of the universal function for nickel system used the first time by Foiles *et al* [6] to compare properties of pure metals. MEAM1NN parameters are those of Ni4 that reproduces the best available experimental results in comparison with Ni1, Ni2 and

Ni3 parameter sets in nickel system in the studies of Baskes [27] and Cherne *et al.* [28] MEAM2NN parameters are taken from Lee *et al's* [14] work. ReaxFF parameters, developed by Zou *et al.*, [17] have been found to give in good agreement with DFT calculations for pure nickel systems.

### 2.2. Kinetic ART

All simulations are performed using the kinetic activation relaxation technique (k-ART) [18,19,29] (Fig. 1), an off-lattice kinetic Monte Carlo method based on the activation relaxation technique (ART nouveau) [30,31] for event searching and the topological analysis package NAUTY [32] for generic classification.

While k-ART is described in more details elsewhere [19,33], the basic algorithm can be summarized in the following steps:

1. Starting with a system relaxed in a local minimum, the local topology associated with each atom is calculated using NAUTY; for Ni, the graph includes all atoms within a 6 Å radius of the central atom, representing around 79 atoms, with vertices drawn between those within 2.6 Å of each other. This connectivity graph is sent to NAUTY which returns a unique identifier characteristic of its automorphic group.
2. If the topology is present in the event catalog, associated events are loaded into the active event list; if not, 50 ART nouveau searches are launched to identify diffusion mechanisms and pathways associated with this topology with additional searches performed for frequently found events to ensure that the catalog is complete. We can assess the completeness of the catalog by comparing events found in independent runs on the same system. In the current work, we find that 50 searches is

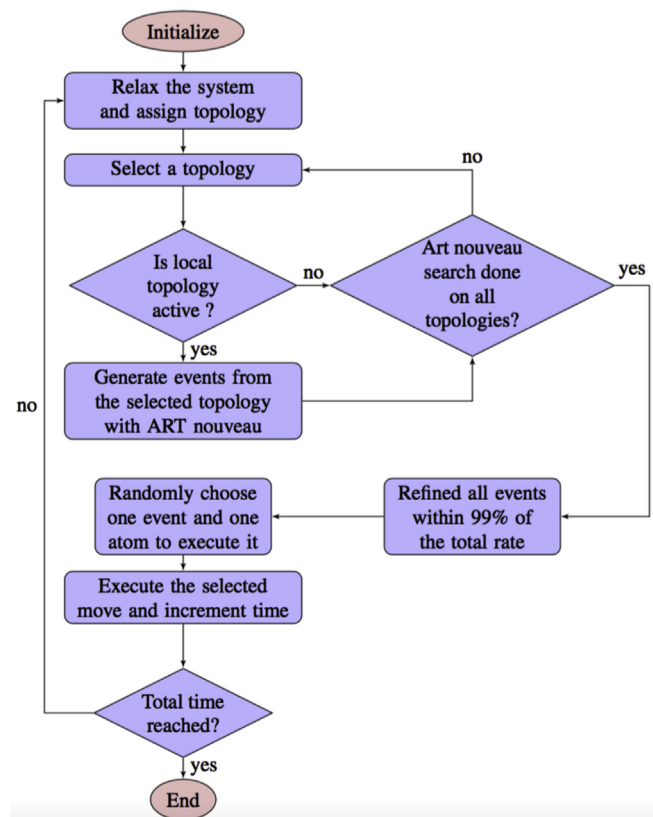


Fig. 1. Kinetic Activation Relaxation Technique (kART) principle.

more than sufficient for all systems except for monovacancy, where we used 100 searches. Not counting events associated with the perfect crystal or with a barrier above 5 eV, a single vacancy in Ni is associated with two events for each potential as it will be indicated later in monovacancy section. In all cases, events are reconstructed to ensure that the saddle point connects two nearby minima.

3. A first evaluation of the KMC timestep is made using the rates of events available for the current conformation. All events with an occurrence probability of 1 in 10 000 or more are then fully reconstructed and their transition state is relaxed to ensure that elastic and configurational effects are exactly taken into consideration. Once this is done, specific rates and the overall KMC timestep are recalculated.
4. A event is selected following the standard KMC algorithm [34], the time and the configuration is updated and the algorithm goes back to step B. Following the standard practice with KMC, a constant pre-exponential factor is used. This approximation was shown to be valid for close-packed metallic systems [35,36].

K-ART provides an extensive representation of the energy landscape surrounding each local minimum, describing in full detail the local activated barriers and connected nearby energy minimums. While this information is essential for constructing a reliable evolution pathway, it also offers a rich view of the system's structure and potential kinetics.

Because it uses an on-the-fly event searching approach and topological classification for cataloging, k-ART can be applied to complex materials and is not restricted to crystalline conformations. Over the last few years, it has been applied to systems such as defects in crystalline metals and semiconductors [22,37], amorphous [20] and ion-bombarded silicon [21,24] and metallic alloys [23].

### 2.3. Simulated system

Vacancies are created by removing atoms from crystalline sites while interstitials are formed by inserting atoms in the central octahedral site of selected fcc cells. All simulations are launched from a fully-relaxed local minimum. Simulations are run for a minimum of 100 and up to 10 000 KMC steps, not including intra-basin jumps, or flickering states, that are resolved analytically using the basin-autoconstructing Mean Rate Method (bac-MRM) [19] built upon Puchala et al.'s Mean-Rate Method [38].

The simulation box is selected after testing convergence on both defect types using EAM potential. Following Ref., [39], convergence is assumed when the energy difference between the first and the last values of formation energy for a specific system in three successive increasing volumes evolves by less than 0.01 eV. A complete table describing this evolution is presented as supplementary material. It shows that even for relatively simple systems such as those studied here, a cubic fcc box of at least a  $9 \times 9 \times 9$  cells (2916 crystalline sites) is necessary to ensure convergence for all systems. In the following, volume is optimized to ensure zero pressure at  $T = 0$  for each potential and simulations are run at  $T = 600\text{K}$ . Since the event catalog is generated at 0 K, the choice of simulation temperature does not affect the list of events, the catalog nor the reconstructed diffusion mechanisms. However, it allows the system to sample by itself a wider range of pathways, making it more straightforward to demonstrate the richness of energy landscape.

### 2.4. Analysis

The formation energy for  $n$  vacancies (v) or interstitials (i) is given by:

$$E_{nv,i}^F = E_{N-n} - \left( E_N \times \frac{N-n}{N} \right) \quad (1)$$

where  $E_N$  is the total energy of a perfect crystalline system with  $N$  nickel atoms and  $E_{N-n}$  is the system's total energy with  $n$  vacancies or interstitials. The binding energy of  $n$  vacancies (v) or interstitials (i) is given by:

$$E_{nv,i}^B = nE_{1v,i}^F - E_{nv,i}^F \quad (2)$$

In all KMC simulations, runs begin with an energy minimization using the Fast Inertial Relaxation Engine (FIRE) method. In these simulations, we use a CPU with a 12-core nodes composed of two processor Intel Westmere-EP X5650 hexa-cores, @2,667 GHz. To give an idea of the speed of the simulation, it takes 7 min, 9.36 h, 16.23 h and 75 h using EAM, MEAM1NN, MEAM2NN and ReaxFF potentials, respectively, with 12 nodes to run 100 k-ART steps in the case of a single vacancy, which corresponds to a simulation time between 0.5 and 8 ms, depending on the exact energy barrier predicted by each potential.

### 2.5. Comparing potentials

Because large simulation cells are required to explore the energy landscape of even small ensembles of self-defects, it is not possible to proceed with *ab initio* description. We therefore compare first the four empirical potentials described above for simple systems for which *ab initio* and experimental results are available: the mono and di-vacancy as well as the self-interstitial.

Monovacancy diffusion is studied with each potential (EAM, MEAM1NN, MEAM2NN and ReaxFF) over 100 k-ART steps, with the complete event catalog obtained before the first step. We obtain the same diffusion mechanisms for all potentials. The vacancy diffuses from a crystalline position to one of the twelve first nearest-neighbor lattice sites by crossing a saddle position situated halfway between nearby lattice sites. The migration and formation energies for this mechanism obviously depend on the specifics of the potentials and are listed in Table 1. As expected we recover the previously calculated formation energies for each potential to within a few 0.01 eV, with the difference largely due to size and convergence effects. Migration barriers associated with first-neighbor jumps are much more precise as finite-size effects are, to first order, the same at the minimum and the transition state.

We also report in Table 1 the energy barriers associated with a direct jump to the second nearest-neighbor sites for the monovacancy. To our knowledge, this mechanism, associated with a high-energy barrier that varies between 4.25 and 4.83 eV depending on the potential, had not been reported previously. Its transition point corresponds to an atom moving by a half-lattice parameter in the  $\langle 100 \rangle$  direction and demonstrates the capacity of k-ART to provide extensive event cataloging.

As also reported in Table 1, DFT calculations and experiments present a range of formation energies for the monovacancy, with EAM and the two MEAM potentials providing values that are between the limits set by DFT and experiments. EAM predicts a formation energy compatible with DFT and within 0.11 eV of the measured value, closest to experimental value of 1.74 eV[34]. ReaxFF, for its part, is 0.3–0.5 eV above DFT and over-estimates the experimental value by 0.18 eV. The monovacancy diffusion barrier energy is found experimentally to be between 1.3 and 1.5 eV[43] compared with the DFT value at the lowest limit (1.29 eV[41]). Here ReaxFF predicts a barrier within the experimental range, 0.06 eV above DFT prediction, while both MEAM potentials are slightly below, at 1.22 eV and EAM under-estimates the barrier by

**Table 1**  
Formation ( $E_{1v}^F$ ), migration for direct vacancy jumps to first ( $E_{1v(1nn)}^m$ ) and activation energies for second ( $E_{1v(2nn)}^a$ ) nearest neighbor sites in nickel. Comparison between values obtained in this work (T.W.) and other works (O.W.) is also presented.

Method	$E_{1v}^F$ (eV)		$E_{1v(1nn)}^m$ (eV)		$E_{1v(2nn)}^a$ (eV)
	T.W.	O.W.	T.W.	O.W.	T.W.
EAM	1.63	1.60[40]	1.07	1.08[6]	4.28
MEAM1NN	1.46	1.48[11]	1.22	1.22[11]	4.44
MEAM2NN	1.56	1.51[14,40]	1.25	–	4.25
ReaxFF	1.92	–	1.35	–	4.83
DFT	–	1.62[41],1.42[42]	–	1.51[41]	–
Experiment	–	1.74[34]	–	1.3–1.5[43]	–

about 0.23 eV.

To further differentiate potentials, we turn to divacancies. Simulations are started with two vacancies distant by 12.2 Å. It takes 34 KMC steps and 95  $\mu$ s using EAM potential to bring the two vacancies in nearest-neighbor position, representing the ground state for this potential. The formation energy in the ground state varies from 2.89 to 3.59 eV depending on the forcefield as indicated in Table 2, in general agreement with DFT predictions that estimate the formation energy to be 2.86 eV [41], except for ReaxFF that overestimates that value by 0.73 eV.

Fig. 3 gives the binding energy as a function of distance for the four potentials, showing two very different behaviors. For MEAM1NN and MEAM2NN, the divacancy is unstable in first and second neighbor positions, with the ground state in fourth neighbor (more stable by 0.36 eV with respect to first neighbor, with a 0.19 eV binding energy). EAM and ReaxFF, for their part, show a more physical and very similar picture, with the binding energy decreasing smoothly with distance and a ground state in first neighbor position, associated with a bonding energy of 0.23 and 0.29 eV, respectively, in agreement with experiment (0.33 eV [44]) and a very slight repulsion at the third and fourth neighbor, with the long-range interactions dying faster for EAM. DFT, for its part, largely underestimates the binding energy of divacancy system with respect to experiment and predicts 0.01 eV in nearest-neighbor position [41]. This mismatch is likely associated with the small 108-atom system used, insufficient to hide the long-range elastic interactions with the PBC images.

Barriers connecting the various configurations are shown in Table 3 for the EAM potential. Similar tables for ReaxFF, MEAM1NN, MEAM2NN potentials are presented in supplementary material. Since MEAM potentials provide the wrong ground state for the divacancy, this defect kinetics is discussed here only for EAM and ReaxFF. The dominant diffusion process for both EAM and ReaxFF is the diffusion by rotation. This latest takes place when one atom diffuses in one of its 1nn vacancy while keeping the divacancies in its ground state. The energy barrier for this mechanism is found to be 0.68 and 0.96 eV for EAM and ReaxFF, respectively.

The four potentials provide the same ground state for the self-interstitial, with the additional atom sharing a site by forming a

**Table 2**  
Diffusion properties of the divacancy in nickel using various potentials. Diffusion coefficient  $D$  and formation energy  $E_{2v}^F$  in the most stable configuration at  $T = 600$  K, with a KMC prefactor of  $10^{13}$  Hz. Diffusion coefficient is calculated from linear regression in the plot of mean square displacement in function of time using Einstein formula  $D = \frac{\langle R^2 \rangle}{6t}$ .

Potential	$D(10^{-10} \text{ cm}^2 \text{ s}^{-1})$	$E_{2v}^F$ (eV)
EAM	4875	3.03
MEAM1NN	0.41	2.89
MEAM2NN	6093	3.29
ReaxFF	3.16	3.59

dumbbell centered on a lattice site with the two atoms positioned at a distance of  $(3/5)a_0$  (2.12 Å) in the  $\langle 100 \rangle$  direction. Formation energy for the four potentials is relatively similar as indicated in Table 4, between 4.21 and 4.78 eV, above the DFT results of 4.07 eV [45]. These latter results are obtained on a 108-atom cell and could be affected by long range elastic effects associated with the insertion of an interstitial in a close-compact network.

These potentials differ, however, in their diffusion pathways. EAM identifies three different mechanisms shown in Fig. 4. In the first mechanism, shown in Fig. 4a A, an atom leaves the dumbbell by jumping to a first neighbor site to form a new dumbbell in a perpendicular direction with respect to the initial dumbbell crossing an energy barrier of 0.14 eV. At the saddle, the diffusing atom is situated in a position between the tetrahedral and octahedral sites. This is in agreement with DFT calculations [45] that show a similar mechanism with an energy barrier of 0.14 eV and with experimental results that estimate the energy barrier for this transition to be 0.15 eV. The second mechanism (B) is similar to the first one but the atom in saddle configuration is situated nearer to the octahedral site with an energy barrier of 0.17 eV. The third diffusion mechanism for the nickel SIA is associated with a saddle point at the octahedral site with a 0.35 eV barrier and it's shown in Fig. 4a C.

ReaxFF, as shown in Fig. 4b B, reproduces EAM's first mechanism where the atom is in the saddle configuration but is situated 0.1 Å closer to the nearest unoccupied octahedron site, with a 0.25 eV barrier, 0.10 eV above DFT and experiments. The second mechanism, shown in Fig. 4b D, is not observed with EAM. It corresponds to a rotation of the dumbbell followed by a shift of one atom of its constructing atom to recreate a dumbbell in the same initial direction but in the nearest position. The energy barrier of this mechanism is high, at 0.59 eV.

Although 1NN and 2NN MEAM forcefields predict elastic constants more precisely than EAM [14], they do not reproduce the single vacancy, divacancy and the self-interstitial energetics accurately when compared with DFT and experiments. EAM and ReaxFF, for their part, show the right overall physics, although they each suffer from some inaccuracies over these three defects. Nevertheless EAM provides surprisingly superior results to ReaxFF. In the rest of the paper, we therefore use EAM for all our calculations.

### 3. Results

We now consider the energy landscape and diffusion mechanisms of vacancy and self-interstitial clusters, with two to five self-defects, using EAM potential.

#### 3.1. Vacancy clusters

Simulations for the two to five vacancies are started with the defects placed at a large enough distance from each other to ensure minimal interaction.

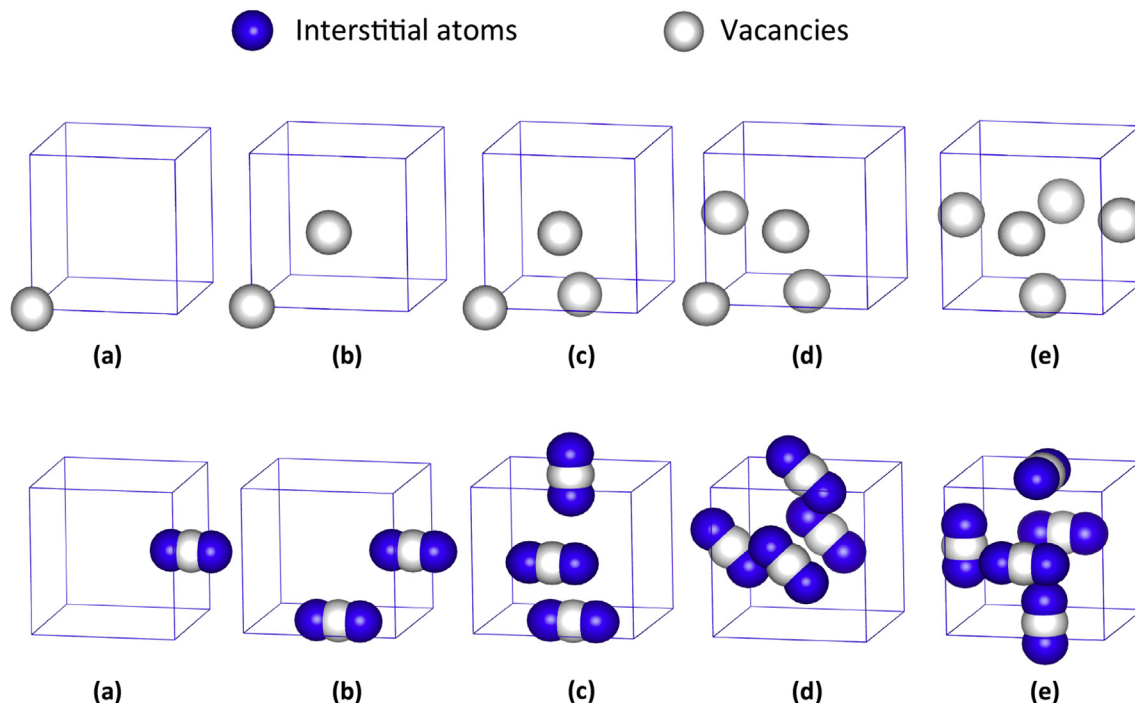


**Fig. 2.** Schematic illustration of lowest-energy states for one to five self-defects in nickel using EAM potential. 1) Ground states for vacancies and 2) self-interstitials. a), b), c), d) and e) present the structure with one, two, three, four and five mono-self-defects for each case.

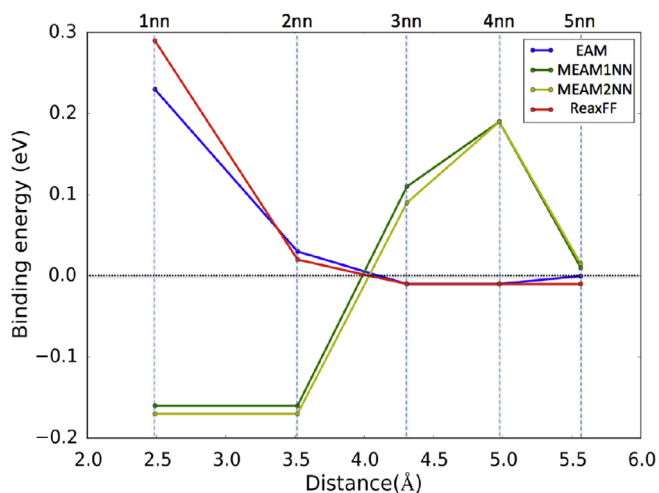


**Fig. 3.** Binding energy for divacancies in nickel as a function of first (1nn) to fifth (5nn) nearest-neighbor distance between vacancies for various potentials.

**Table 3**

Relative configuration ( $\Delta E$ ) and barrier energies for pathways between the five dominant bound states for the divacancy complex using EAM potential ( $x$  nn). All barriers are associated with an atom jumping over a 1nn distance, except for the barrier labeled with an asterisk (\*) for which the jump is to 2nn. Energies are in eV.

To	From				
	1nn	2nn	3nn	4nn	5nn
$\Delta E$	0	0.20	0.23	0.23	0.23
1nn	0.68	1.03	0.89	0.87	–
2nn	1.23	–	1.01	–	1.07
3nn	1.11, 4.40*	1.04	1.05	1.01	–
4nn	1.10	–	1.01	–	1.07
5nn	–	1.07	–	1.07	–

As discussed above, vacancy pairs form rapidly into dimers with the two point defects at a first nearest-neighbor distance from each other. From the ground state, the dominant diffusion mechanism, with a 0.68 eV barrier, is a rotation that involves migration of one atom in a nearest-neighbor site while keeping the dimer in 1nn conformation (1nn-dimer), in agreement with experimental results and DFT calculations [41]. Divacancies can also diffuse through pure translation, where a vacancy migrates to a nearest-neighbor site forming a dimer of vacancies in third neighbor position (3nn-dimer) with a 1.11 eV barrier. This conformation is metastable, 0.23 eV above the ground state, and reforms into a 1nn-dimer crossing a 0.89 eV barrier. From the 3nn-dimer, reconstruction of the 1nn-dimer is the most probable move (see Table 3) as the barrier further separating the vacancies is 1.01 eV, implying a probability of 91% at  $T = 600$  K to reform the 1nn-dimer. Other less probable breaking mechanisms going through an intermediate 2nn-dimer are also possible. A detailed description of the energetics of the rotation and translation mechanisms is given in Fig. 5 with the transition details between the first five states provided in Table 3.

The three isolated vacancies aggregate to form the ground state in 0.25 ms and 190 KMC steps, with the three vacancies in first neighbor (1nn) position, forming an equilateral triangle as indicated in Fig. 2. This cluster is characterized by a binding energy of 0.68 eV (0.23 eV per vacancy) as measured from the three isolated vacancies. Since divacancy diffusion is faster than the monovacancy, the initial formation of a dimer is relatively slow (taking 0.14  $\mu$ s). Once a divacancy is formed, it rapidly finds its way to the remaining monovacancy.

Due to fcc symmetry, the trivacancy cluster can diffuse through rotation of the cluster, with one vacancy jumping to a first neighbor site, without breaking the triangle, crossing a barrier of only 0.35 eV. The cluster is stable and can be broken only by crossing barriers of 0.84 and 0.86 eV, corresponding to jumps of one of the vacancies into 3nn and 2nn position, respectively, as measured

**Table 4**Formation and migration energies of 1SIA in nickel using different potentials. The considered formation energy is relative to  $\langle 100 \rangle$  dumbbell. Energies are in eV.

Method	Formation energy (eV)		Migration energy (eV)	
	This work	Other works	This work	Other works
EAM	4.54	5.05[6]	0.14	0.14[6]
MEAM1NN	4.37	4.24[27]	0.18	0.28[27]
MEAM2NN	4.21	4.88[14]	0.27	–
ReaxFF	4.78	–	0.25	–
DFT	–	4.07[45]	–	0.14[46], 0.15[47], 0.18[40]
Experiment	–	–	–	0.15[48], 0.16[49]

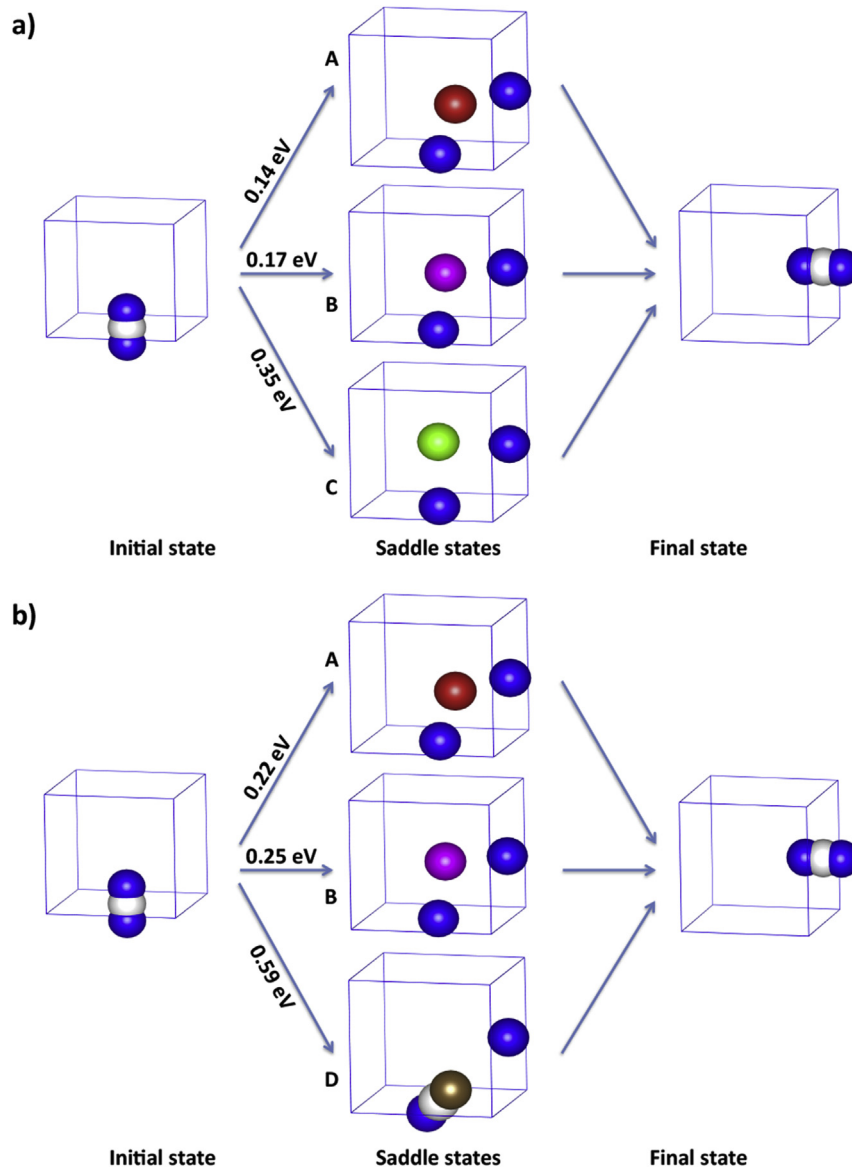


**Fig. 4.** Mono-self-interstitial of nickel diffusion mechanisms using a) EAM and b) ReaxFF potentials. A,B,C,D are the possible saddles for each mechanism. A: the atom is in a position between the octahedron and tetragonal sites (This state is obtained by both EAM and ReaxFF potentials with energy barriers of 0.14 and 0.25 eV, respectively). B: same as for A but the atom is nearest to the octahedron site. C: the saddle configuration as the diffusing atom is in the octahedron position. D: the dumbbell turns in the  $\langle 111 \rangle$  direction before rotating and shifting to create a new dumbbell in the same initial direction and in nearest neighbor site. The interstitial atom is indicated in white at the minimum position and various colors at the saddle. Ni atoms in crystalline position are in blue. (For interpretation of the references to colour in this figure legend, the reader is referred to the web version of this article.)

from the remaining divacancy. Along these less probably pathways, the trivacancy complex diffuses by transiting between ground and excited states situated at 0.23 and 0.19 eV above the fundamental

state. Fig. 6 shows the diffusion in time of the center of mass for the trivacancy system.

K-ART also identifies a high energy state, 0.4 eV above the

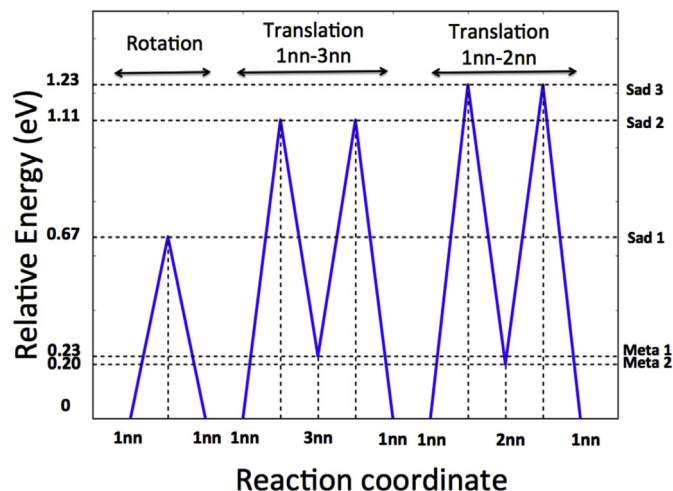


**Fig. 5.** Dominant diffusion mechanisms for divacancies in nickel. Energies for saddle points (sad1, sad2 and sad3) and meta-stable (meta1 and meta2) are shown in figure for each mechanism. Rotation takes place through a one-step mechanism moving one atom by a 1nn distance to a 1nn vacancy site. Translation takes place through the diffusion of one atom into a 1nn vacancy site forming dimer of vacancies in 3nn and 2nn distance. The diffusion of a second atom then reforms a dimer of vacancies in 1nn.

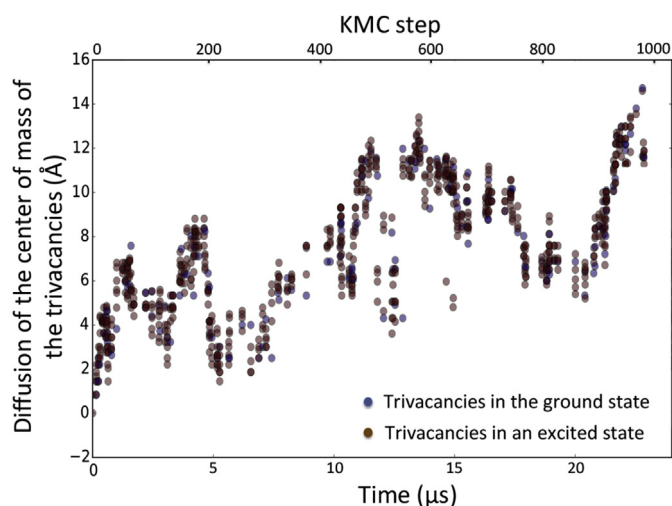


**Fig. 6.** Center of mass diffusion as a function of time for trivacancies in Ni. Diffusion and time are measured from the position of the first occurrence of ground state. Blue and brown symbols corresponds to trivacancies in fundamental and excited states respectively. (For interpretation of the references to colour in this figure legend, the reader is referred to the web version of this article.)

ground state, that corresponds to a tetrahedron of vacancies surrounding a displaced atom, for the three vacancy system. This state is unstable and requires crossing only a 0.08 eV barrier to move back to the ground state. This state is interesting as it was observed by Dilpuneet *et al* in a Ni system run at 1000 K using MD and a different EAM parameter set [50], suggesting a higher stability than what is found with k-ART, although it is not clear from that work whether this defect plays an important role at these temperatures. To understand this apparent contradiction, we launched a series of MD simulations in the NPT ensemble and at zero pressure to check the stability of this defect at temperatures from 300 to 1000 K, in 50 K steps. We find that the tetrahedron defect is, indeed, unstable at temperatures below 400 K and that, as lattice vibrations become important, entropic contributions stabilize the defect, significantly increasing its lifetime.

Starting from four isolated vacancies, the ground state for the tetravacancy is reached in about 4  $\mu$ s and 102 KMC steps. Aggregation occurs in steps, with the formation a rapidly diffusing divacancy that absorbs a third vacancy, with the cluster moving to the remaining vacancy consecutively. The ground state is characterized by four vacancies forming a regular tetrahedron with edges of 1nn distance between each pair of vacancies as indicated in Fig. 2. Binding energy for the ground state, as measured from four isolated vacancies, is 1.36 eV, or 0.34 eV per vacancy.

The shortest diffusion mechanism for the tetravacancy complex is described in Fig. 7. Diffusion takes place in four steps by the migration of one vacancy that jumps to 1nn positions at each step. The first jump is energetically expensive with a barrier of 1.07 eV; with such high barrier, the tetravacancy ground state is largely a pinning center with a two microseconds diffusion timescale at 600 K. Once this barrier is crossed, the diffusion goes on rapidly crossing barriers of 0.26, 0.51 and 0.64 eV to a new ground state situated in another corner of the Ni unit cell as indicated in Fig. 7.

A second important diffusion mechanism for tetravacancy system includes the same initial transition as in the first mechanism. The system then jumps to higher energy state leading to four vacancies further than that in the first mechanism in the second step, crossing a 0.70 eV of energy barrier that brings the system to a state 0.20 eV above the ground state, corresponding to the second excited state in the tetravacancy system. With two successive inverse transitions to those in the two second steps, the ground tetrahedron is reformed. The migration barrier associated with mechanism is equal to 1.13 eV.

Due to the complexity of the tetravacancy diffusion mechanisms and the low mobility of the monovacancy, the aggregation into a pentavacancy of five isolated vacancies is relatively a slow process. Since the energy landscape for both the monovacancy and tetravacancy systems have been explored, we therefore start the exploration of this more complex system with the five vacancies already aggregated. The ground state (GS) for this system forms an equilateral pentahedron in (100) direction with a square base and an edge of 1nn distance and 2nn length for the diagonals, with a binding energy of 1.91 eV or 0.38 eV per atom (Fig. 2). As in the case

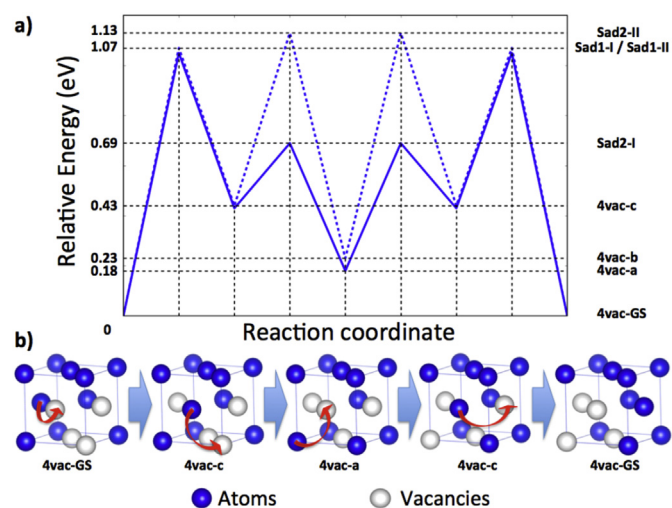


**Fig. 7.** Tetravacancy diffusion mechanism in nickel from ground state. a) Energy landscape for the dominant (continuous blue line I) and the second diffusion mechanisms (dotted blue line II). b) Atomistic representation of the dominant diffusion mechanism. States 4vac-GS, 4vac-a, 4vac-b, 4vac-c are ordered from the most to the least stable states along the pathway. Red arrows indicated the changes between conformations. (For interpretation of the references to colour in this figure legend, the reader is referred to the web version of this article.)

of tetravacancies, diffusion takes place by a successive migrations of one vacancy into a 1nn crystalline position. The first move, from the ground state, requires crossing a 0.58 eV energy barrier. The shortest diffusion mechanism, described in Fig. 8, takes approximately 5 ns. This mechanism allows the diffusion of the fundamental pentahedron through a rotation into a new direction as defined by a line passing from the center of mass and the summit of the cluster. This mechanism diffuses the pentavacancy system by about 1.97 Å in around 2 ns.

A second mechanism, with a 0.66 eV of energy barrier, is related to the migration of the atom which is symmetric to the summit of the pentahedron through the base to one of its vacancy sites. This mechanism is non diffusive but leads to a same-cell rotation of the pentahedron into to a new perpendicular  $\langle 100 \rangle$  direction.

A 5-step diffusion mechanism is also observed. A 1nn atom in the parallel plane to the base of the pentahedron and passing from summit first migrates to the summit, after crossing a barrier of 0.71 eV, leading to a deformed pentahedron. This state is situated at 0.50 eV from the GS. Then, by crossing a barrier of 0.21 eV to reach the first excited state of this system (0.29 eV from the GS). Starting from this configuration, the four vacancies cross a symmetric barrier of 0.56 eV, leading to an overall migration barrier of 0.85 eV.

A number of mechanisms with energy barriers higher than 0.97 eV are also found but, being rare, they are not discussed here.

### 3.2. Self-interstitial clusters

We now turn to systems counting from two to five SIA to explore diffusion processes as a function of cluster size.

#### 3.2.1. Di-self-interstitial

Simulation of the two self-interstitial (SIA) system is started with the defects separated by 4.98 Å corresponding to the distance between fourth nearest neighbors in crystalline fcc nickel. These defects come rapidly in close contact and in less than 0.4 ps reach the ground state corresponding to the formation of two parallel  $\langle 100 \rangle$  (or equivalent) dumbbells in nearest neighbor position.

Fig. 9 presents the three most frequent diffusion mechanisms for the 2SIA system. The dominant one takes place over three steps through the  $\langle 110 \rangle$  configuration, following the crowdion motion as

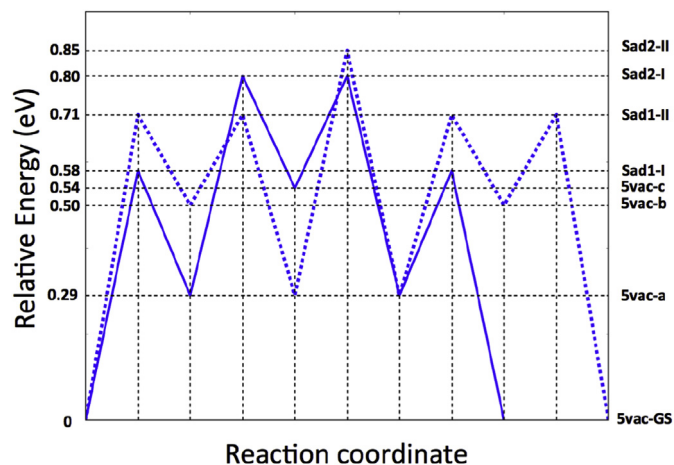


Fig. 8. Pentavacancy diffusion mechanisms in nickel from the ground state. Energy landscape for the shortest mechanism (continuous blue line and index I) and the second diffusion mechanism (dotted blue line and index II). States 5vac-GS, 5vac-a, 5vac-b, 5vac-c are ordered from the most to the least stable states along the pathway. (For interpretation of the references to colour in this figure legend, the reader is referred to the web version of this article.)

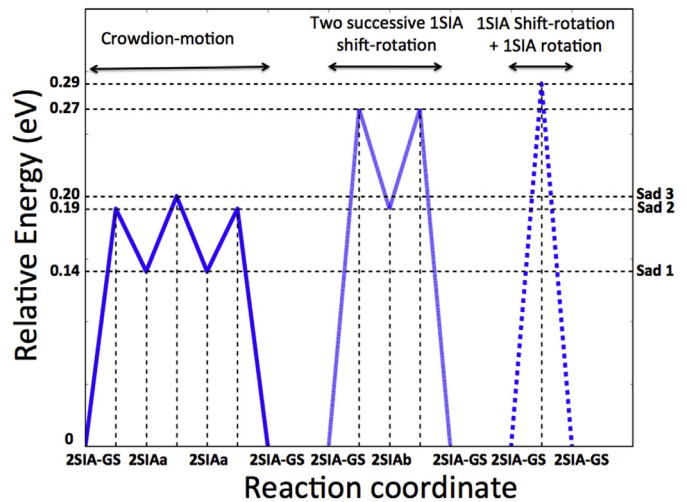


Fig. 9. The three dominant diffusion mechanisms for 2SIA in nickel. The first two states above the ground state (2SIA-GS) are referred to as 2SIAa and 2SIAb, respectively. GS corresponds to two parallel dumbbells oriented along the  $\langle 100 \rangle$  direction (or equivalent) in 1nn position. In 2SIAa, the dumbbells are parallel in the  $\langle 110 \rangle$  direction (or equivalent) in 1nn position and 2SIAb is associated with the dumbbells in 1nn position but perpendicular to each other in  $\langle 110 \rangle$  directions.

reported in Zhao's *et al* work [49]: First, a simultaneous rotation of the two dumbbells from the  $\langle 100 \rangle$  GS to a  $\langle 110 \rangle$  orientation is achieved by crossing a barrier of 0.19 eV characterized by the two dumbbells turned  $22.5^\circ$  from the  $\langle 100 \rangle$  direction. Going over a second barrier, at 0.06 eV, the dimer jumps to a nearby site, maintaining its  $\langle 110 \rangle$  orientation and then can relax into the ground state through a 0.05 eV barrier. This diffusion mechanism is in agreement with Zhao et al.'s [49] 0.12 eV barrier.

K-ART also identifies a second low-energy diffusion mechanism, with a 0.27 eV barrier, that moves the 2SIA by two successive 1SIA shift-rotations leading to the ground state again. At 600 K, and considering the fact that there is 24% of probability to cross a single 0.20 eV barrier, this mechanism should occur about 12% of the time.

A third low-energy diffusion mechanism with a barrier of 0.29 eV is also observed. This mechanism takes place in only one step with a dumbbell rotating in perpendicular position versus as the other makes a 1SIA shift-rotation to reconstruct the 2SIA-GS as a final configuration. At 600 K, this mechanism should still occur about 17% of the time.

Rarer mechanisms, with barriers of 1.3 eV and higher, are also identified but, given their very low probability, are not discussed here.

The 3SIA simulation starts with two interstitials 4.98 Å apart and the third one 9.96 Å away from the first two. We find that the most stable configuration for the 3SIA system in nickel is when the dumbbells are all in first nearest neighbor, except for one dumbbell where the distance is equal to 2nn, with two parallel and the third one perpendicular to them in  $\langle 100 \rangle$  and equivalents as indicated in Fig. 2. This configuration is reached after 31 KMC steps from the beginning of the simulation, corresponding to 0.37 ps. The dominant diffusion process for this system, with a 0.14 eV barrier, takes place by a crowdion motion as in the case of 2SIA by translation after rotation from the  $\langle 100 \rangle$  to  $\langle 110 \rangle$  direction for the three dumbbells as reported in Zhao's *et al* work [49]. Fig. 10 shows the configurations associated with the 3SIA. Seven of them are found to dominate, representing more than 96% of all accepted configurations. The most important state is the 3SIAb involved in the dominant diffusion mechanism with a barrier of 0.05 eV as indicated in Table 5. The 3SIAb-3SIAb transition is related to the

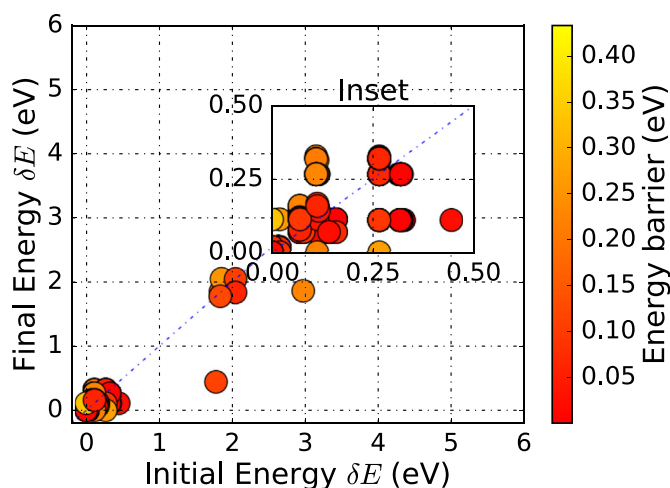


**Fig. 10.** Representation of all k-ART accepted activation events for the tri-self-interstitial atoms system for a 1000 KMC steps simulation. All initial and final energies are measured from 3SIA-GS, the ground state. Inset: zoom-in between 0 and 0.50 eV. Symbols are color-coded according to the scale on the right. (For interpretation of the references to colour in this figure legend, the reader is referred to the web version of this article.)

**Table 5**

Relative configuration energies (E) (top line) and barrier energies for pathways between the five dominant bound states for the 4SIA system. Energies are in eV.

To	From			
	3SIA-GS	3SIAa	3SIAb	3SIAc
$\Delta E$	0	0.02	0.06	0.08
3SIA-GS	0.14	0.06	0.29	0.27
3SIAa	0.08	0.13	0.54	–
3SIAb	0.37	0.60	0.05	–
3SIAc	0.38	–	–	–

crowdion motion corresponding to a diffusion following the  $\langle 110 \rangle$  direction. The transitions between 3SIA-GS and 3SIAa and conversely, with barriers of 0.08 and 0.06 respectively, are not a diffusion mechanism but result in a change in the dumbbells' orientation.

Starting at distances between 7.04 Å and 12.19 Å or each other, the four interstitials aggregate after 28 KMC steps and 62 ns.

The most stable configuration for 4SIA places all the dumbbells in the  $\langle 110 \rangle$  direction or equivalents and in 1nn distance except for one pair with a 2nn distance as indicated in Fig. 11. The formation energy for 4SIA-GS is equal to 12.08 eV or 3.02 eV per SIA. The binding energy connecting dumbbells forming the 4SIA-GS cluster is equal to 5.99 eV or 1.50 eV per atom.

The diffusion kinetics of the 4SIA-GS structure system is dominated by very low-barrier mechanism, only 0.004 eV, which is in a good agreement with MD-simulation result [49]. This low barrier in comparison with that of other transitions indicated in Table 6 implies that only this diffusion mechanism, which is related to the crowdion motion as reported in Zhao's [49] work, will be selected predominantly.

The five interstitials are placed initially at distances between 10.56 Å to 15.23 Å. They aggregate and reach the ground state after 0.5 ns (24 KMC steps). Once aggregated, the pentavacancy cluster diffuses quickly. The 5SIA ground state corresponds to the five dumbbells all within 1nn distance except for two pairs in 2nn position, distributed in different equivalent  $\langle 100 \rangle$  directions and a binding energy of 7.67 eV or 1.53 eV per atom. The GS and the three first excited states of 5SIA are presented in Fig. 11 and are identified

5SIA-GS, 5SIAa, 5SIAb and 5SIAc from the most to the least stable configuration, respectively. States 5SIAa and 5SIAb are very close in energy but are not the same, as is shown in the supplementary material.

While the GS is characterized by close dumbbells distributed in  $\langle 100 \rangle$  directions (and equivalents), excited states place all dumbbells in  $\langle 110 \rangle$  directions. Transition barriers between these states are shown in Table 7. Since dumbbells in 5SIA-GS and the other are distributed differently, transitions between the ground and one of the excited states require a collective movement of all dumbbells either by rotation or translation or both, which explain the 0.61-eV barrier found for this system, much higher than for one to three SIA. Once relaxed into excited state, diffusion takes place easily by transiting between different states. The most dominant diffusion mechanism is the crowdion motion corresponding to the 5SIAa-5SIAa transition with an energy barrier of 0.09 eV, in agreement with those mentioned by Zhao *et al* [49]. Transitions between 5SIAa and 5SIAc with low energy barriers and movement of only one dumbbell are non diffusive mechanisms and corresponds to an oscillations between these two states. Diffusion along  $\langle 100 \rangle$  direction is slow and requires a high activation barrier at least 1.09 eV as indicated in Table 7. Despite being a simple system, with only 5SIA, k-ART was able to identify hundreds of barriers relating only the four considered states. In the case of GS-GS transition, for example, k-ART identifies 9 possible barriers corresponding to different mechanisms that ranges from 1.09 eV to 3.25 eV.

#### 4. Discussion and conclusion

Points defects play an important role in determined the properties of materials [1,2,25] and understanding how they aggregate and move through crystals remain a major challenge as experimental approaches fail to provide the necessary detailed microscopic information. Direct calculations can compensate experimental limitations in the case of simple point defects but the rapidly increasing complexity of the energy landscape of even small clusters requires automated search tools that have become available only relatively recently [51].

Following the characterization of points defects in bcc iron [22,51] we turned to fcc systems, looking at the energy landscape associated with crystalline Ni containing one to five vacancies and self-interstitials to identify trends in defects diffusion and aggregation. To ensure the relevance of this study, we first compared four empirical potentials — EAM [6], MEAM1NN [27,28], MEAM2NN [14] and ReaxFF [17] — with experimental and *ab initio* results for simple defects, one and two vacancies and one self-interstitial. While both MEAM potentials describe incorrectly the di-vacancy energetics, ReaxFF and EAM are in generally good agreement with experiment and DFT calculations. Overall, EAM provides the best accord, although it underestimates the mono-vacancy diffusion barrier by 20–25% and is the potential we used for the characterization of points defects in Ni.

We describe in detail the energy landscape of one to five vacancy clusters, finding a non-monotonic diffusion rate as a function of size. As for k-ART study of bcc Fe [22], we find that the tri-vacancy diffuses particularly rapidly, with a barrier of only 0.35 eV, compared to 0.68 and 1.07 eV, for the di and tetravacancy clusters, due to the underlying crystalline symmetry that allows the cluster to move directly from ground state to ground state. While pentavacancy cluster diffusion is much slower than tetravacancy in Fe, it is the opposite in fcc Ni, with an overall diffusion barrier lower by about 0.27 eV pentavacancy. The overall energy landscape for vacancies in fcc system, however, appears to be much richer than for bcc, likely due to the local environment surrounding these point defects.

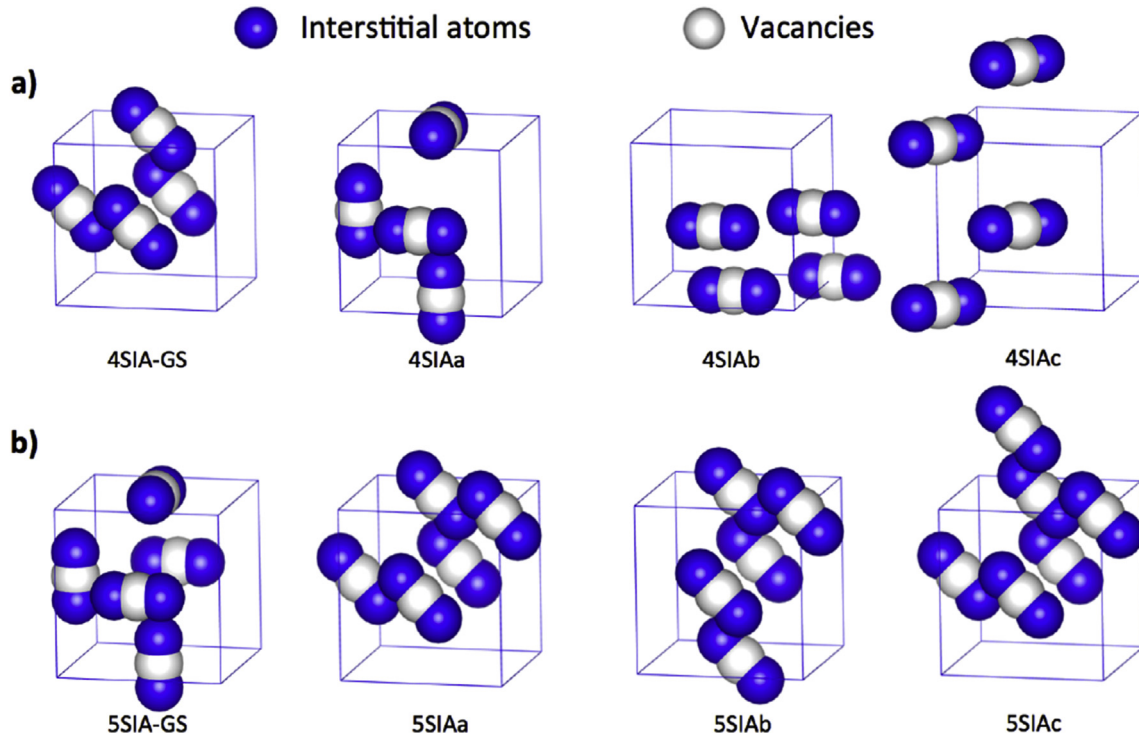


Fig. 11. Most stable configurations for a) four and b) five SIA in nickel. Indices a to d reference to configurations ordered starting from the most stable state for each system.

Table 6

Relative configuration ( $\Delta E$ ) (top line) and barrier energies for pathways between the five dominant bound states for the 4SIA system. Indexes refer to the number of active dumbbells in the diffusion process (for example  $0.92_{2d}$  means diffusion with an energy barrier of 0.92 eV in which two dumbbells are moving). Energies are in eV.

To	From			
	4SIA-GS	4SIAa	4SIAb	4SIAC
$\Delta E$	0	0.62	0.83	0.91
4SIA-GS	0.00 $_{4sd}$ , 0.89 $_{4d}$ , 1.27 $_{4d}$	0.31 $_{4d}$	0.14 $_{4d}$	–
4SIAa	0.93 $_{4d}$	1.46 $_{4d}$	–	–
4SIAb	0.90 $_{4d}$	–	–	–
4SIAC	0.92 $_{2d}$	–	–	–

Table 7

Relative configuration ( $E$ ) (top line) and barrier energies for pathways between the five dominant bound states for the 5SIA system. Indexes means the number of moved dumbbells in the diffusion process. Energies are in eV.

To	From			
	5SIA-GS	5SIAa	5SIAb	5SIAC
$\Delta E$	0	0.04	0.06	0.12
5SIA-GS	1.09 $_{2d}$ , 2.13 $_{4d}$ , 3.25 $_{5d}$	0.56 $_{5d}$	0.16 $_{5d}$	0.59 $_{5d}$
5SIAa	0.61 $_{5d}$	0.09 $_{5d}$	1.55 $_{5d}$	0.03 $_{1d}$ , 4.36 $_{4d}$
5SIAb	0.23 $_{5d}$	1.57 $_{5d}$	0.56 $_{2d}$	–
5SIAC	0.71 $_{5d}$	0.11 $_{1d}$ , 4.40 $_{4d}$	–	–

Even though diffusion occurs on widely different time scale for various clusters, it is often accompanied by a change in the diffusion direction and can involve many steps. The fastest diffusion pathway for tetra and pentavacancy clusters, for example, requires crossing four barriers associated with as many single vacancy jumps. This suggests that the 1D vacancy cluster diffusion observed in Au by Matsukawa and Zinkle requires much larger clusters to set in than studied here [52].

Interstitial diffusion in compact lattices is complex, with the number of barriers and mechanisms increasing rapidly with the number of self-defects [51]. For fcc metals, simulations have shown that small self-interstitial clusters diffuse very rapidly along the  $\langle 110 \rangle$  direction, although details of these mechanisms were not provided [25,49]. With k-ART, it is possible to reconstruct in detail the energy landscape surrounding the various clusters. While the diffusion barrier for a single interstitial is already low, at 0.15 eV, it drops to 0.08 eV for the 3SIA cluster and even to 0.004 eV for 4SIA, essentially ensuring a free diffusion across the crystal, with the help of the crowdion mechanism, which involves a collective rotation of dumbbells, from the  $\langle 100 \rangle$  to the  $\langle 110 \rangle$ , followed by a jump in the same direction. As the cluster size increases, this collective rotation from the ground state into an excited state becomes costlier, as observed already for the 5SIA cluster, which requires crossing a 0.61 eV barrier to realign all dumbbells. From this point, however, diffusion remains very rapid, with barriers of 0.09 eV. Since the fast diffusing state is only 0.04 eV above the GS, its occurrence probability is high. This suggest a similar behavior for larger SIA clusters, where the ground state might gain in stability but with fast diffusing excited states with a sufficiently life-time to dominate SIA kinetics, explaining experimental observations for this type of defects [25,53]. The picture that emerges for SIA diffusion in simple fcc metals appears more straightforward than that observed in bcc Fe, where diffusion barriers for small SIA clusters increase with cluster size and are associated with fairly complicated moves [51] in spite of a similar richness in terms of number of available states.

Using k-ART, we have provided here a detailed characterization of point defect clustering for system counting from one to five vacancies and self-interstitials. These results represent a strong basis to further work at relating these mechanisms with results obtained on larger clusters that involve important mechanisms such as stacking fault tetrahedra [50,54] that occur for clusters with more than 5 vacancies and can greatly affect the mechanical properties of metals. As shown experimentally, self-defect diffusion

is largely influenced not only by the crystalline lattice but also by the nature of the alloys. Interstitials, for examples, diffuse much more slowly in NiFe and even pure Fe than in pure Ni, while vacancies gain in diffusivity. Much work remains to understand these differences. Extensive methods, such as k-ART, make it possible, at last, to turn our attention to these systems.

### Code availability

Various ART nouveau implementations are available freely for download from <http://normandmousseau.com>. The k-ART code is available from the authors upon request.

### Acknowledgments

This work has been supported by the Canada Research Chairs program and by grants from the Natural Sciences and Engineering Research Council of Canada (NSERC) and the Fonds Québécois de la Recherche sur la Nature et les Technologies (FQRNT). We are grateful to Calcul Quebec for generous allocations of computer resources.

### Appendix A. Supplementary data

Supplementary data related to this article can be found at <https://doi.org/10.1016/j.actamat.2017.11.021>.

### References

- [1] P.G. Klemens, Thermal resistance due to point defects at high temperatures, *Phys. Rev.* 119 (2) (1960) 507.
- [2] R. Gul, U.N. Roy, S.U. Egariyevwe, A.E. Bolotnikov, G.S. Camarda, Y. Cui, A. Hossain, G. Yang, R.B. James, Point defects: their influence on electron trapping, resistivity, and electron mobility-lifetime product in cdxte<sub>se</sub>1-x detectors, *J. Appl. Phys.* 119 (2) (2016) 025702.
- [3] I.J. Robertson, M.C. Payne, K-point sampling and the K P method in, *J. Phys. Condens. Matter* 2 (1990) 9837.
- [4] W.L. Jorgensen, J. Chandrasekhar, J.D. Madura, R.W. Impey, M.L. Klein, Comparison of simple potential functions for simulating liquid water, *J. Chem. Phys.* 79 (2) (1983) 926–935.
- [5] M.S. Daw, M.I. Baskes, Embedded-atom method: derivation and application to impurities, surfaces, and other defects in metals, *Phys. Rev. B* 29 (12) (1984).
- [6] S.M. Foiles, M.I. Baskes, M.S. Daw, Embedded-atom-method functions for the fcc metals Cu, Ag, Au, Ni, Pd, Pt, and their alloys, *Phys. Rev. B* 33 (12) (1986) 7983–7991.
- [7] J.H. Rose, J. Ferrante, J.R. Smith, Universal binding energy curves for metals and bimetallic interfaces, *Phys. Rev. Lett.* 47 (9) (1981) 675–678.
- [8] M.I. Baskes, Application of the embedded-atom method to covalent materials: a semiempirical potential for silicon, *Phys. Rev. Lett.* 59 (23) (1987) 2666–2669.
- [9] M.I. Baskes, J.S. Nelson, A.F. Wright, Semiempirical modified embedded-atom potentials for silicon and germanium, *Phys. Rev. B* 40 (9) (1989) 6085–6100.
- [10] M.I. Baskes, Modified embedded-atom potentials for cubic materials and impurities, *Phys. Rev. B* 46 (5) (1992) 2727–2742.
- [11] M.I. Baskes, R.A. Johnson, Modified embedded atom potentials for HCP metals, *Model. Simul. Mater. Sci. Eng.* 2 (1) (1999) 147–163.
- [12] B.J. Lee, M.I. Baskes, Second nearest-neighbor modified embedded-atom-method potential, *Phys. Rev. B* 62 (13) (2000) 8564–8567.
- [13] B.J. Lee, M.I. Baskes, Hanchul Kim, Yang Koo Cho, Second nearest-neighbor modified embedded atom method potentials for bcc transition metals, *Phys. Rev. B* 64 (18) (2001).
- [14] B.J. Lee, J.H. Shim, M. Baskes, Semiempirical atomic potentials for the fcc metals Cu, Ag, Au, Ni, Pd, Pt, Al, and Pb based on first and second nearest-neighbor modified embedded atom method, *Phys. Rev. B* 68 (14) (2003) 1–11.
- [15] A.C.T. Van Duin, S. Dasgupta, F. Lorant, W.A. Goddard, ReaxFF: a reactive force field for hydrocarbons, *J. Phys. Chem. A* 105 (41) (2001) 9396–9409.
- [16] M.P. Ariza, R. Serrano, J. P. Mendez, M. Ortiz, Stacking faults and partial dislocations in graphene, *Philos. Mag.* 92 (16) (2012) 2004–2021.
- [17] C. Zou, Y.K. Shin, A.C.T. van Van Duin, H. Fang, Z.K. Liu, Molecular dynamics simulations of the effects of vacancies on nickel self-diffusion, oxygen diffusion and oxidation initiation in nickel, using the ReaxFF reactive force field, *Acta Mater.* 83 (2015) 102–112.
- [18] F. El-Mellouhi, N. Mousseau, Laurent J. Lewis, Kinetic activation-relaxation technique: an off-lattice self-learning kinetic Monte Carlo algorithm, *Phys. Rev. B* 78 (15) (2008) 153202.
- [19] L.K. Béland, P. Brommer, F. El-Mellouhi, J.F. Joly, N. Mousseau, Kinetic activation-relaxation technique, *Phys. Rev. E* 84 (4) (2011) 1–11.
- [20] J.F. Joly, L.K. Béland, P. Brommer, F. El-Mellouhi, N. Mousseau, Optimization of the kinetic activation-relaxation technique, an off-lattice and self-learning kinetic monte-carlo method, *J. Phys. Conf. Ser.* 341 (012007) (2012).
- [21] L.K. Béland, N. Mousseau, Long-time relaxation of ion-bombarded silicon studied with the kinetic activation-relaxation technique: microscopic description of slow aging in a disordered system, *Phys. Rev. B* 88 (21) (2013).
- [22] P. Brommer, L.K. Béland, J.F. Joly, N. Mousseau, Understanding long-time vacancy aggregation in iron: a kinetic activation-relaxation technique study, *Phys. Rev. B* 90 (13) (2014) 1–9.
- [23] O.A. Restrepo, N. Mousseau, F. El-Mellouhi, O. Bouhali, M. Trochet, C.S. Becqar, Diffusion properties of Fe-C systems studied by using kinetic activation-relaxation technique, *Comput. Mater. Sci.* 112 (2016) 96–106.
- [24] A. Jay, M. Raine, N. Richard, N. Mousseau, V. Goiffon, A. Hemeryck, P. Magnan, Simulation of single particle displacement damage in silicon Part II: generation and long time relaxation of damage structure, *IEEE Trans. Nucl. Sci.* 64 (1) (2017) 141–148.
- [25] C. Lu, L. Niu, N. Chen, K. Jin, T. Yang, P. Xiu, Y. Zhang, F. Gao, H. Bei, S. Shi, M.R. He, I. Robertson, W.J. Weber, L. Wang, Enhancing radiation tolerance by controlling defect mobility and migration pathways in multicomponent single phase alloys, *Nat. Commun.* 7 (2016) 1–8.
- [26] S. Plimpton, Fast parallel algorithms for short  $\delta$  range molecular dynamics, *J. Comput. Phys.* 117 (June 1994) (1995) 1–19.
- [27] M.I. Baskes, Determination of modified embedded atom method parameters for nickel, *Mater. Chem. Phys.* 50 (2) (1997) 152–158.
- [28] F. Cherne, M.I. Baskes, P. Deymier, Erratum: properties of liquid nickel: a critical comparison of EAM and MEAM calculations, *Phys. Rev. B* 66 (14) (2002) 1–9.
- [29] M. Trochet, A. Sauvé-Lacoursière, N. Mousseau, Algorithmic developments of the kinetic activation-relaxation technique: accessing long-time kinetics of larger and more complex systems, *J. Chem. Phys.* 147 (15) (2017) 152712.
- [30] G.T. Barkema, N. Mousseau, Event-based relaxation of continuous disordered systems, *Phys. Rev. Lett.* 77 (21) (1996) 4358.
- [31] R. Malek, N. Mousseau, Dynamics of lennard-jones clusters: a characterization of the activation-relaxation technique, *Phys. Rev. E* 62 (2000) 7723–7728.
- [32] B.D. McKay, Practical Graph Isomorphism, Department of Computer Science, Vanderbilt University Tennessee, US, 1981.
- [33] N. Mousseau, L.K. Béland, P. Brommer, F. El-Mellouhi, J.F. Joly, G.K. N'tsouaglo, O.A. Restrepo, M. Trochet, Following atomistic kinetics on experimental timescales with the kinetic Activation Relaxation Technique, *Comput. Mater. Sci.* 100 (2015) 111–123.
- [34] A.B. Bortz, M.H. Kalos, J.L. Lebowitz, A new algorithm for Monte Carlo simulation of Ising spin systems, *J. Comput. Phys.* 17 (1) (1975) 10–18.
- [35] Handan Yildirim, Abdelkader Kara, Talat S. Rahman, Origin of quasi-constant pre-exponential factors for adatom diffusion on cu and ag surfaces, *Phys. Rev. B* 76 (16) (2007) 165421.
- [36] H. Chamati, N.I. Papanicolaou, Y. Mishin, D.A. Papaconstantopoulos, Embedded-atom potential for fe and its application to self-diffusion on fe (100), *Surf. Sci.* 600 (9) (2006) 1793–1803.
- [37] M. Trochet, L.K. Béland, J.F. Joly, P. Brommer, N. Mousseau, Diffusion of point defects in crystalline silicon using the kinetic activation-relaxation technique method, *Phys. Rev. B* 91 (22) (2015) 224106.
- [38] B. Puchala, M.L. Falk, K. Garikipati, An energy basin finding algorithm for kinetic monte carlo acceleration, *J. Chem. Phys.* 132 (13) (2010) 134104.
- [39] P. Korzhavyi, I. Abrikosov, B. Johansson, A. Ruban, H. Skriver, First-principles calculations of the vacancy formation energy in transition and noble metals, *Phys. Rev. B* 59 (18) (1999) 11693–11703.
- [40] E. Asadi, M.A. Zaeem, A. Moitra, M.A. Tschopp, Effect of vacancy defects on generalized stacking fault energy of fcc metals, *J. Phys. Condens. Matter Inst. Phys. J.* 26 (11) (2014) 115404.
- [41] E.H. Megchiche, C. Mijoule, M. Amarouche, First principles calculations of vacancy-vacancy interactions in nickel: thermal expansion effects, *J. Phys. Condens. Matter* 22 (48) (2010) 485502.
- [42] P. Kumar Nandi, M.C. Valsakumar, S. Chandra, H.K. Sahu, C.S. Sundar, Efficacy of surface error corrections to density functional theory calculations of vacancy formation energy in transition metals, *J. Phys. Condens. Matter* 22 (34) (2010) 345501.
- [43] H. Bakker, A curvature in the  $\ln d$  versus  $1/T$  plot for self-diffusion in nickel at temperatures from 980 to 1400°C, *Phys. Status Solidi (b)* 28 (2) (1968) 569–576.
- [44] H. Kronmüller, in: A. Seeger, D. Schumacher, W. Schilling, J. Diehl (Eds.), Vacancies and Interstitials in Metals, North-Holland Publ. Co., Amsterdam, 1970.
- [45] J.D. Tucker, T.R. Allen, D. Morgan, Ab initio defect properties for modeling radiation-induced segregation in Fe-Ni-Cr alloys, in: 13th Environmental Degradation of Materials in Nuclear Power Systems, January 2015, p. 2007.
- [46] S.T. Howard, Ab initio 10 (1996) 6085–6090.
- [47] D. Connétable, É. Andrieu, D. Monceau, First-principles nickel database: energetics of impurities and defects, *Comput. Mater. Sci.* 101 (2015) 77–87.
- [48] S. Nanaot, K. Kuribayashig, S. Tanigawall, and M. Doyamall, Studies of defects at thermal equilibrium and melting in Cu and Ni by positron annihilation ? 1403.
- [49] P. Zhao, Y. Shimomura, Molecular dynamics calculations of properties of the self-interstitials in copper and nickel, *Comput. Mater. Sci.* 14 (1–4) (1999) 84–90.
- [50] Dilpuneet S. Aidhy, Chenyang Lu, Ke Jin, Hongbin Bei, Yanwen Zhang,

- Lumin Wang, William J. Weber, Formation and growth of stacking fault tetrahedra in ni via vacancy aggregation mechanism, *Scr. Mater.* 114 (2016) 137–141.
- [51] M.-C. Marinica, F. Willaime, N. Mousseau, Energy landscape of small clusters of self-interstitial dumbbells in iron, *Phys. Rev. B* 83 (9) (2011) 1–14.
- [52] Y. Matsukawa, Steven J. Zinkle, Where N, *Science* 318 (November) (2007) 959–962.
- [53] A.S. Dilpuneet, C. Lu, K. Jin, H. Bei, Y. Zhang, L. Wang, W.J. Weber, Point defect evolution in Ni, NiFe and NiCr alloys from atomistic simulations and irradiation experiments, *Acta Mater.* 99 (Complete) (2015) 69–76.
- [54] Enrique Martínez, Blas P. Uberuaga, Mobility and coalescence of stacking fault tetrahedra in cu, *Sci. Rep.* 5 (2015).